Cancer Science

WILEY | JCA JAPANESE CANCER ASSOCIATION

ORIGINAL ARTICLE OPEN ACCESS

Liposomal ^{188}Rhenium Plus Macrophage Depletion Enhances Anti-PD-L1 Efficacy and B Cell Infiltration Against Lung Metastatic Cancer

Shin-Yi Liu[1,2] | Liang-Ting Lin[3] | Chih-Hsien Chang[4] | Yu-Jen Chen[5,6,7]

[1]Department of Biomedical Imaging and Radiological Science, China Medical University, Taichung, Taiwan | [2]Graduate Institute of Biomedical Sciences, China Medical University, Taichung, Taiwan | [3]Department of Health Technology and Informatics, The Hong Kong Polytechnic University, Kowloon, Hong Kong | [4]Department of Isotope Application Research, National Atomic Research Institute, Taoyuan, Taiwan | [5]Department of Medical Research, China Medical University Hospital, Taichung, Taiwan | [6]Department of Radiation Oncology, MacKay Memorial Hospital, Taipei, Taiwan | [7]Department of Medical Research, MacKay Memorial Hospital, New Taipei City, Taiwan

Correspondence: Chih-Hsien Chang (chchang@iner.gov.tw) | Yu-Jen Chen (chenmdphd@gmail.com)

Received: 2 August 2025 | **Revised:** 10 September 2025 | **Accepted:** 12 September 2025

Funding: This work was supported by Taitung MacKay Memorail Hospital, TTMMH-112-02, TTMMH-110-02; Mackay Memorial Hospital, MMH-E-114-11, MMH-E-113-11, MMH-E-111-11; China Medical University Hospital, CMU109-N-26; National Science and Technology Concil, Taiwan, MOST 109-2314-B-039-059.

Keywords: B cells | liposome | macrophages | PD-L1 | Rhenium-188

ABSTRACT

Radionuclides such as Rhenium-188 (Re188) hold promise for treating metastatic cancers due to their cytotoxic effects and potential to stimulate systemic anti-tumor immunity. However, mononuclear phagocyte system-mediated clearance of liposome encapsulated Re188 (Lipo-Re188) limits its tumor delivery. This study aimed to enhance the therapeutic effect of Lipo-Re188 against lung metastases through macrophage depletion and immune checkpoint blockade. A lung metastatic colon cancer model was established via intravenous injection of CT26-luciferase cells and then treated with Lipo-Re188 (11.1 MBq, 30% of MTD), liposomal clodronate (Lipo-clod) for macrophage depletion, and/or anti-PD-L1 antibody. Tumor progression was monitored by bioluminescence imaging, and radionuclide biodistribution was assessed at 1, 24, and 48 h post-injection. Flow cytometry was used to assess immune cell populations in the spleen and tumor microenvironment (TME). Cytokine levels were measured using a bead-based multiplex assay and analyzed by flow cytometry. Macrophage depletion significantly enhanced tumor accumulation of Lipo-Re188 while reducing hepatic uptake and prolonging survival. The combination of Lipo-clod and Lipo-Re188 promoted B cells, restored functional T cells, and suppressed MDSC in both spleen and TME. Notably, IL-1α and GM-CSF levels were significantly elevated in the combination group. Triple therapy with Lipo-clod, Lipo-Re188, and anti-PD-L1 provided the greatest survival benefit, highest intratumoral B cell accumulation, and lowest interstitial macrophage levels, with no significant biological toxicity. Our study reveals that triple therapy overcomes immunosuppressive feedback and promotes a tumor-suppressive microenvironment. These findings support a rational combination strategy integrating radiopharmaceutical therapy with immune modulation for metastatic cancer treatment.

Abbreviations: CT26-luc, CT26 cells stably expressing luciferase; EPR, enhanced permeability and retention; ICI, immune checkpoint inhibitors; Lipo-clod, liposome encapsulated clodronate; Lipo-Re188, liposome encapsulated Rhenium-188; MDSC, myeloid-derived suppressor cells; MPS, mononuclear phagocyte system; MTD, maximum tolerated dose; TME, tumor microenvironment.

1 | Introduction

Administration of radionuclides allows systemic delivery of ionizing radiation, enabling not only direct targeting of disseminated tumor cells but also modulation of systemic immunity [1, 2]. Liposome-encapsulated radionuclide is a widely employed strategy in drug delivery systems for applications in cancer therapy, autoimmune disorders, and regenerative medicine [3–6]. The lipid bilayer of liposomes provides structural protection for therapeutic agents, including nucleotides, and serves as a versatile platform for antibody conjugation and surface modification, enabling targeted delivery [7–9]. Rhenium-188 (Re188) is a promising theranostic radionuclide for malignant tumor treatment, owing to its favorable characteristics, including a moderate half-life (16.9 h), high β-particle emission energy (2.11 MeV), adequate tissue penetration range (~11 mm), and a cost-effective generator-based production system [10–12]. In addition to its therapeutic capabilities, Re188 emits both β-particles and γ-rays, making it amenable to imaging and biodistribution tracking. Liposome-encapsulated Re-188 (Lipo-Re188) has been developed to improve tumor-specific delivery and therapeutic outcomes, and its efficacy has been demonstrated in preclinical models of head and neck, lung, liver, pancreatic, ovarian, and colon cancers [13–16]. Lipo-Re188 accumulates in the tumor microenvironment (TME) via the enhanced permeability and retention (EPR) effect—characterized by abnormal vasculature, impaired lymphatic drainage, and elevated interstitial pressure—and delivers localized β-radiation to cancer cells [17–19]. Moreover, Re188-labeled molecules—including peptides, antibodies, Lipiodol, and particulates—have been evaluated in early-phase clinical trials, such as primary tumors, bone metastases, rheumatoid arthritis, and endovascular interventions [20–23].

The immunological impact of radionuclide therapy is increasingly recognized as a determinant of therapeutic efficacy and is influenced by factors such as radiation type, dose, delivery kinetics, and the immune composition of the TME [24, 25]. In tumors, radiation induces immunogenic cell death (ICD), which promotes the release of damage-associated molecular patterns (DAMP), activation of the stimulator of interferon genes (STING) pathway, and upregulation of MHC class I molecules. These events support antigen presentation and dendritic cell activation, ultimately promoting $CD8^+$ T cell priming and systemic anti-tumor immunity [26–28]. Additionally, radiation can reshape systemic cytokine milieus—elevating IFN-β, IL-6, and TNF-α—which facilitate immune cell recruitment and activation [25, 29]. However, sublethal radiation may also transiently alter the balance of immune subsets, including T cells, NK cells, regulatory T cells (Tregs), and myeloid-derived suppressor cells (MDSC), thereby influencing both immunostimulatory and immunosuppressive responses [30, 31]. MDSC consist of two main subsets: polymorphonuclear MDSC (PMN-MDSC), which share phenotypic and functional features with neutrophils, and monocytic MDSC (M-MDSC), which resemble monocytes. Both subsets exert strong immunosuppressive effects and collectively constitute one of the most potent cell populations limiting T-cell activation and effector function within the TME. Collectively, radionuclide therapy not only delivers therapeutic irradiation to tumors but also initiates a cascade of systemic immune events that can overcome immune resistance in metastatic cancer.

Compared to free Re188, Lipo-Re188 demonstrates markedly different pharmacokinetics, biodistribution, and immunologic interactions [32]. Lipo-Re188 exhibits prolonged systemic circulation, increased tumor accumulation, and preferential uptake by the mononuclear phagocyte system (MPS) [33]. The MPS—comprising liver Kupffer cells, splenic macrophages, and bone marrow phagocytes—plays a pivotal role in liposome clearance, representing a major barrier to effective delivery of liposomal radiotherapeutics [34]. High MPS uptake raises concerns regarding off-target radiation exposure, hepatotoxicity, splenic dysfunction, and perturbations in systemic cytokine balance [35–37]. Uptake by the MPS is influenced by liposomal physicochemical properties, such as size, surface charge, and opsonization [38, 39]. PEGylated nanoscale liposomes (~100 nm) offer advantages by reducing phagocytic uptake and enhancing tumor-specific extravasation [40, 41]. Nevertheless, intracellular decay of radionuclides within MPS macrophages may impair phagocytic function and immune homeostasis, potentially exacerbating immunotoxicity during repeated treatments. Current literature on the immune regulatory effects of liposomal radionuclide therapies remains limited, and the underlying mechanisms and clinical implications are yet to be clearly defined.

In this study, we employed a combination strategy of low-dose PEGylated Lipo-Re188 and macrophage depletion via liposomal clodronate (Lipo-clod) to modulate Lipo-Re188 biodistribution and reduce hepatic toxicity. By attenuating MPS-mediated clearance, we hypothesized that Lipo-Re188 accumulation in the TME would increase, enhancing therapeutic efficacy. However, Lipo-clod treatment has been reported to elevate circulating neutrophils [42–44], which may limit anti-tumor efficacy due to high PD-L1 expression on neutrophils. To overcome this, we further implemented PD-L1 immune checkpoint blockade as a third therapeutic component. This study provides a mechanistic understanding of how liposomal radionuclide therapy modulates systemic and local immunity and highlights rational combination strategies to maximize efficacy while minimizing off-target effects.

2 | Material and Methods

2.1 | Cell Culture

The murine colorectal adenocarcinoma cell line CT26 was obtained from the American Type Culture Collection (ATCC, Manassas, VA, USA) and maintained in RPMI-1640 medium (Gibco, Thermo Fisher Scientific, Waltham, MA, USA) supplemented with 10% heat-inactivated fetal bovine serum (FBS; HyClone, Logan, UT, USA), 2 mM L-glutamine under standard culture conditions (37°C, 5% CO_2). For in vivo bioluminescence imaging, stable luciferase-expressing clones (CT26-luc) were generated with a lentiviral vector encoding the North American Firefly luciferase genes and selected using 400 μg/mL G418 (Geneticin; Sigma-Aldrich, St. Louis, MO, USA).

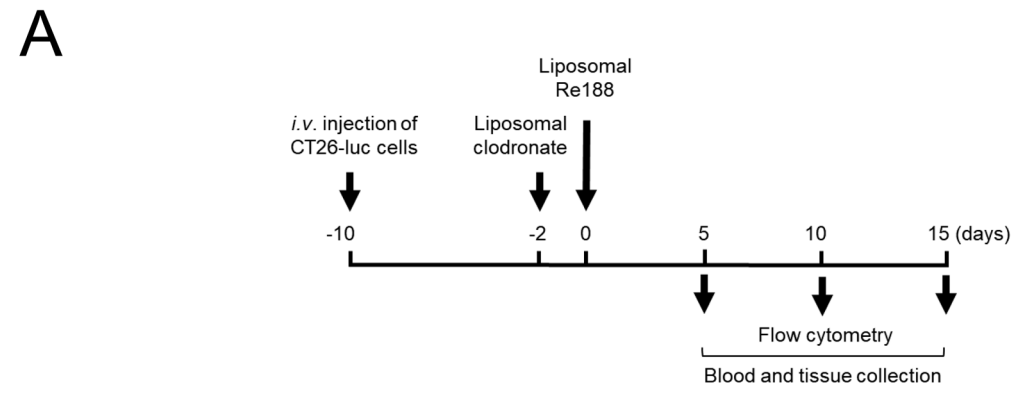

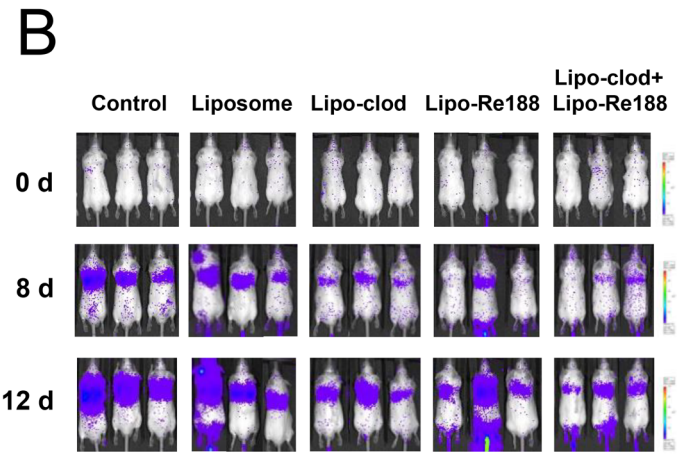

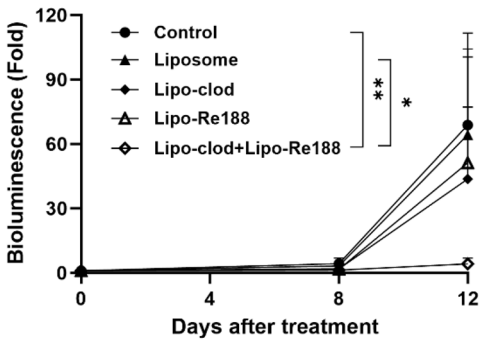

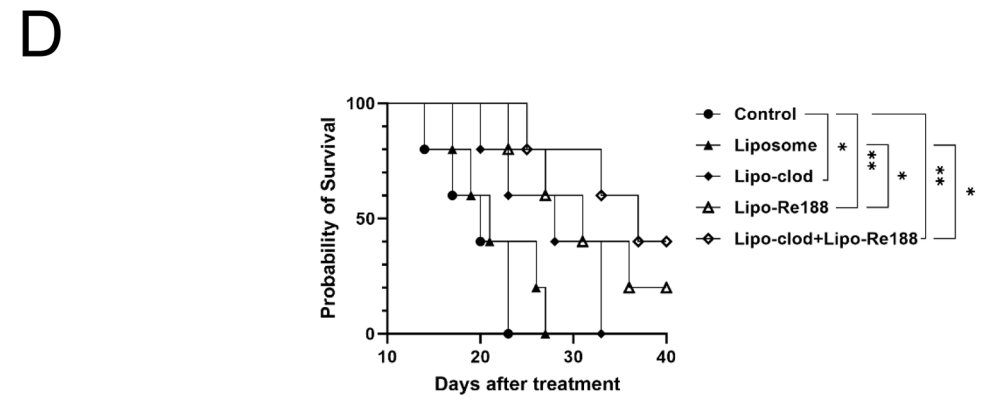

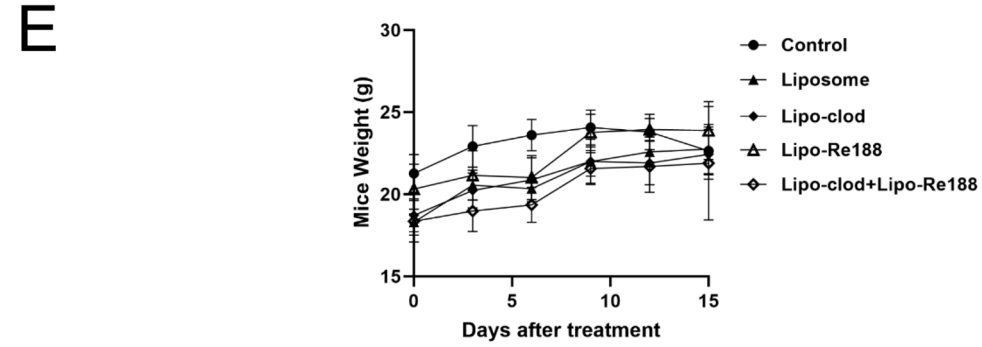

FIGURE 1 | Macrophage depletion enhances anti-tumor efficacy of Lipo-Re188 in lung metastatic cancer mice. (A) Schematic of the experimental design. CT26-luc lung metastasis-bearing mice were randomized into five treatment groups: Untreated control, liposome, liposomal clodronate (Lipo-clod), liposomal Rhenium-188 (Lipo-Re188), and combination therapy (Lipo-clod+Lipo-Re188). (B) Representative IVIS images showing lung tumor burden on days 0, 8, and 12 post-treatment ($n = 3$). (C) Quantification of lung tumor burden based on total photon flux within the lung region of interest (ROI) ($n = 3$). (D) Kaplan–Meier survival analysis of all treatment groups ($n = 5$). Assessment of systemic toxicity: Body weight (E), white blood cell count (F), alanine aminotransferase (ALT) (G), and creatinine (CRE) (H) levels during the 15-day post-treatment ($n = 5$). Data are presented as mean ± SD. Statistical significance was determined by one-way ANOVA with Tukey's multiple comparisons test or log-rank test for survival. $^{*}p < 0.05$; $^{**}p < 0.01$.

2.2 | Preparation of PEGylated Liposomal Re188

Nano-X PEGylated liposomes (average diameter: 82.59 nm; Taiwan Liposome Company, Taipei, Taiwan) were composed of hydrogenated soy phosphatidylcholine (HSPC), cholesterol, and DSPE-PEG2000 in a molar ratio of 3:2:0.3. The internal aqueous phase of the liposomes contained 250 mM ammonium sulfate (pH 5.0). The total phospholipid concentration was 13.16 mM, as determined by the phosphate quantification assay. Re-188 was obtained by eluting a carrier-free $^{188}W/^{188}Re$ generator (IRE, Fleurus, Belgium) with sterile saline to produce sodium perrhenate ($NaReO_4$). The radionuclide was chelated with N,N-bis(2-mercaptoethyl)-N′,N′-diethylenediamine (BMEDA; ABX, Radeberg, Germany) in the presence of sodium gluconate and stannous chloride. Briefly, 3 mg of BMEDA was mixed with 0.34 M sodium gluconate in 10% acetate solution, followed by the addition of 0.02 M stannous chloride dihydrate (Merck, Darmstadt, Germany). The Re188 solution was added and incubated at 80°C for 1 h. Radiolabeling efficiency was assessed using instant thin-layer chromatography on silica gel (ITLC-SG) with normal saline as the mobile phase (Rf: Re188 = 0.8–1.0; Re188-BMEDA = 0.0–0.2). Prior to liposomal loading, the pH of the Re188-BMEDA complex was adjusted to 7.0 with 2 N NaOH. The radiolabeled complex was incubated with PEGylated liposomes at 60°C for 30 min to facilitate encapsulation. Free Re188-BMEDA was separated using a PD-10 desalting column (GE Healthcare, Chicago, IL, USA), and radiolabeling efficiency was calculated as the percentage of radioactivity associated with liposomes after separation. Lipo-Re188 exhibited a radiochemical purity of 98.5%, specific activity of 63.2 MBq/μmol, particle size of 83.7 nm, zeta potential of −1.1 mV, and plasma stability of 88.03% at 24 h, as previously reported [21, 45].

2.3 | Experimental Animal Model

Male BALB/c mice (4 weeks old) were purchased from the National Laboratory Animal Center (Taipei, Taiwan). All experimental procedures were approved by the Institutional Animal Care and Use Committee (MMH-A-S-108-25) of Mackay Memorial Hospital and conformed to institutional and international guidelines for animal welfare. To establish a lung metastasis model, 1×10^6 CT26-luc cells suspended in 50 μL PBS were injected into the tail vein of each mouse. Tumor development was monitored using the IVIS Spectrum imaging system (PerkinElmer, Waltham, MA, USA) following intraperitoneal injection of D-luciferin (150 mg/kg; GoldBio, St. Louis, MO, USA). Mice exhibiting comparable luminescent signals on day 7 post-inoculation were randomized into treatment groups. Liposomal clodronate (Lipo-clod; 2 μm; Encapsula NanoSciences, Brentwood, TN, USA) was administered via tail vein injection at a dose of 50 mg/kg 2 days prior to radionuclide administration. Mice received a single intravenous injection of Lipo-Re188 at a subtherapeutic dose of 11.1 MBq (30% of maximum tolerated dose; 100 μL per mouse). For combination immunotherapy, anti-PD-L1 monoclonal antibody (clone 10F.9G2; Bio X Cell, Lebanon, NH, USA) was administered intraperitoneally at 7.5 mg/kg on days 0, 2, and 4 following Lipo-Re188 treatment. Mice were monitored for body weight, white blood cells, liver and kidney functions, and survival throughout the study.

2.4 | Bio-Distribution of Liposomal Re188

Lung metastatic mice bearing CT26-luc cells were intravenously injected with 2.22 MBq of Lipo-Re188 with and without liposomal clodronate treatment. The mice were sacrificed by CO_2 asphyxiation, and organs of interest were removed, washed, and weighed at 1, 24, and 48 h post-injection. The radioactivity of Lipo-Re188 was detected using an Auto-Gamma counter (Packard Cobra II, Canberra, Germany), and data were expressed as the percentage of injected dose per gram of tissue (% ID/g).

2.5 | Hemogram and Biochemistry

White blood cell (WBC) counts were measured using a hematology analyzer (HEMAVET HV950; Drew Scientific, Dallas, TX, USA). Plasma was isolated by centrifugation at 2000 ***g*** for 10 min and used for biochemical analyses. Aminotransferase (ALT) and creatinine (CRE) levels were determined using Fuji Dri-Chem slide assays (Fujifilm, Tokyo, Japan) according to the manufacturer's protocol.

2.6 | Flow Cytometry Analysis

Mice were euthanized by ketamine (100 mg/kg) and xylazine (10 mg/kg) intramuscularly. Spleens and lungs were harvested and enzymatically digested using collagenase A (1.5 mg/mL) and DNase I (0.4 mg/mL) for 30 min at 37°C. Cell suspensions were filtered through 70 μm strainers, and red blood cells were lysed using ACK buffer. Following Fc block with anti-CD16/CD32 (BD Biosciences), cells were stained with a panel of fluorochrome-conjugated monoclonal antibodies (BioLegend, San Diego, CA, USA) for 20 min on ice. The following antibody-fluorochrome conjugates were used: anti-CD3-Alexa Fluor 488, anti-NKG2D-PE, CD11c-PE/Dazzle594, anti-Siglec F-PerCP/Cy5.5, anti-Ly6G-PE/Cy7, PD-1-APC, anti-F4/80-APC/Cyanine7, anti-Ly6C-Brilliant Violet 421, anti-CD45-Brilliant

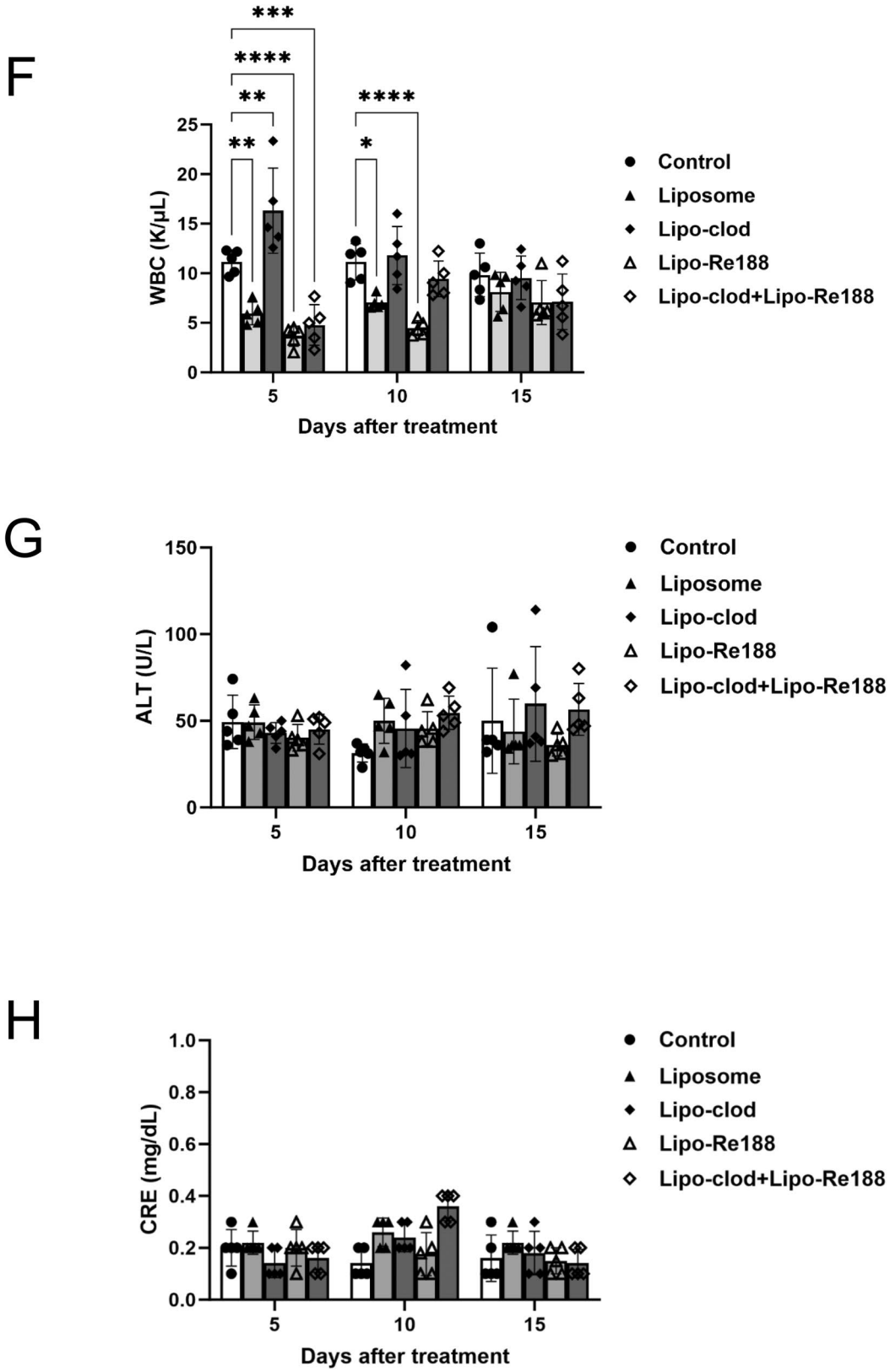

FIGURE 1 | (Continued)

Violet 510, anti-CD11b-Brilliant Violet 605, anti-MHCII-Brilliant Violet 650, and anti-CD8-Brilliant Violet 785 (BioLegend, San Diego, CA, USA). After washing, cells were immediately analyzed using the CytoFLEX 13-color cytometer (Beckman Coulter, Brea, CA, USA) and quantified using CytExpert analysis software. Immune subsets were defined as: PMN-MDSC ($CD11b^+/Ly6G^+$), M-MDSC ($CD11b^+/Ly6C^{++}$), $CD4^+$ T cells ($CD11b^-/CD3^+/CD8^-$), $CD8^+$ T cells ($CD11b^-/CD3^+/CD8^+$), NKT cells ($CD11b^-/CD3^+/NKG2D^+$), natural killer cells ($CD3^-/MHCII^-/NKG2D^+$), B cells ($CD11b^-/MHCII^+/CD11c^-$),

TABLE 1 | Bio-distribution of liposomal Rhenium-188 with or without macrophage depletion.

Lipo-Re188	1 h		24 h		48 h	
Lipo-clod	−	+	−	+	−	+
Brain	1.14 ± 0.24	0.97 ± 0.26	0.32 ± 0.07	0.48 ± 0.11*	0.17 ± 0.05	0.40 ± 0.10*
Heart	4.19 ± 1.19	4.57 ± 1.56	2.26 ± 0.64	2.22 ± 0.44	1.43 ± 0.44	3.13 ± 0.91*
Lung	8.28 ± 1.17	6.25 ± 0.62*	3.92 ± 0.53	4.73 ± 0.58	2.36 ± 0.46	5.11 ± 1.03**
Liver	9.17 ± 2.13	4.97 ± 4.49	11.45 ± 3.70	4.29 ± 1.11*	9.82 ± 2.04	4.98 ± 1.23*
Stomach	1.31 ± 0.19	1.26 ± 0.26	1.46 ± 0.47	1.16 ± 0.28	1.20 ± 0.26	1.54 ± 0.22
Small Intestine	4.49 ± 1.36	4.11 ± 0.70	5.47 ± 2.60	4.08 ± 1.01	5.22 ± 1.58	7.22 ± 1.43
Large intestine	1.80 ± 1.06	1.60 ± 0.69	2.90 ± 0.65	1.85 ± 0.55	2.18 ± 1.09	2.81 ± 0.36
Pancreas	1.87 ± 0.61	1.98 ± 0.12	1.00 ± 0.18	1.09 ± 0.30	0.61 ± 0.12	1.69 ± 0.52*
Spleen	8.06 ± 0.61	34.61 ± 12.54*	12.20 ± 1.99	28.78 ± 7.48*	12.53 ± 5.12	36.67 ± 4.24**
Kidney	8.92 ± 1.67	6.87 ± 1.78	5.85 ± 0.87	5.66 ± 1.05	4.04 ± 0.65	7.86 ± 1.89*
Testis	0.48 ± 0.03	0.45 ± 0.08	0.28 ± 0.02	0.33 ± 0.04	0.20 ± 0.09	0.37 ± 0.06*
Muscle	0.62 ± 0.18	0.45 ± 0.09	0.40 ± 0.07	0.35 ± 0.19	0.17 ± 0.03	0.22 ± 0.03*
Skin	0.77 ± 0.14	0.47 ± 0.12*	1.22 ± 0.44	0.61 ± 0.16*	1.06 ± 0.28	1.62 ± 0.78
Bone	0.29 ± 0.11	0.43 ± 0.22	0.25 ± 0.08	0.37 ± 0.13	0.10 ± 0.02	0.09 ± 0.03**
Bone marrow	0.38 ± 0.11	0.71 ± 0.20*	0.62 ± 0.24	0.89 ± 0.35	0.25 ± 0.15	0.42 ± 0.17
Urine	6.55 ± 3.46	16.71 ± 4.94*	6.97 ± 3.62	3.04 ± 2.51	1.15 ± 1.05	2.76 ± 1.05
Blood	23.29 ± 2.72	38.37 ± 13.22	11.61 ± 3.49	14.05 ± 2.81	2.94 ± 0.61	9.80 ± 1.27***
Feces	4.57 ± 3.62	3.68 ± 5.00	13.69 ± 12.25	4.96 ± 1.35	4.54 ± 2.95	4.04 ± 1.88
Tumor/Muscle	13.35	13.89	9.8	13.51	13.89	23.22

Note: Values are expressed as percentages of injected dose per gram (% ID/g ± SD). Statistical analysis was performed between the liposomal clodronate-treated group and the non-treated group by a two-tailed Student's *t*-test at each time point ($n = 3$).
*$p < 0.05$; **$p < 0.01$; ***$p < 0.001$.

splenic macrophages ($CD11b^m/MHCII^+/F4/80^+$), alveolar macrophages ($CD11b^m$/Siglec F^+/ $CD11c^+$), interstitial macrophages ($CD11b^+/MHCII^+/F4/80^+$), dendritic cells ($MHCII^+/CD11c^+$), and eosinophils ($CD11b^+$/Siglec $F^+/F4/80^+$).

2.7 | Cytokine Detection

Plasma cytokines were quantified using the LEGENDplex Mouse Inflammation Panel (13-plex; BioLegend) according to the manufacturer's instructions. The panel included IL-23, IL-1α, IFN-γ, TNF-α, MCP-1, IL-12p70, IL-1β, IL-10, IL-6, IL-27, IL-17A, IFN-β, and GM-CSF. Samples were analyzed on a CytoFLEX 13-color cytometer, and data were processed using LEGENDplex analysis software.

2.8 | Statistical Analysis

Data were analyzed using GraphPad Prism (GraphPad Software, San Diego, CA, USA). Results are expressed as mean ± standard deviation (SD). For comparisons between two groups, unpaired *t*-tests were used for normally distributed data, while the Mann–Whitney *U* test was applied for non-parametric data. For multiple comparisons, one-way ANOVA with Tukey's post hoc test was used when variance assumptions were met; otherwise, Welch's ANOVA or Kruskal–Wallis test with Dunn's correction was applied. Survival data were analyzed using the log-rank (Mantel–Cox) test. A *p*-value < 0.05 was considered statistically significant.

3 | Results

3.1 | Macrophage Depletion Enhances Therapeutic Efficacy of Lipo-Re188

To enhance the therapeutic index and reduce off-target effects of liposomal radionuclide therapy, we employed a macrophage depletion strategy using liposomal clodronate (Lipo-clod). A lung metastatic model was established via intravenous injection of CT26-luciferase (CT26-luc) colon cancer cells. Tumor burden was assessed using an in vivo imaging system (IVIS) on day 7 post-injection, and mice were randomized into six groups: normal (no tumor), metastatic control, liposome, Lipo-clod, Lipo-Re188, and Lipo-clod + Lipo-Re188 combination. Based on our previous findings, the maximum tolerated dose (MTD) of Lipo-Re188 in BALB/c mice was 37 MBq [46]. For this study, a single intravenous dose of 11.1 MBq (30% of the MTD) in 100 μL

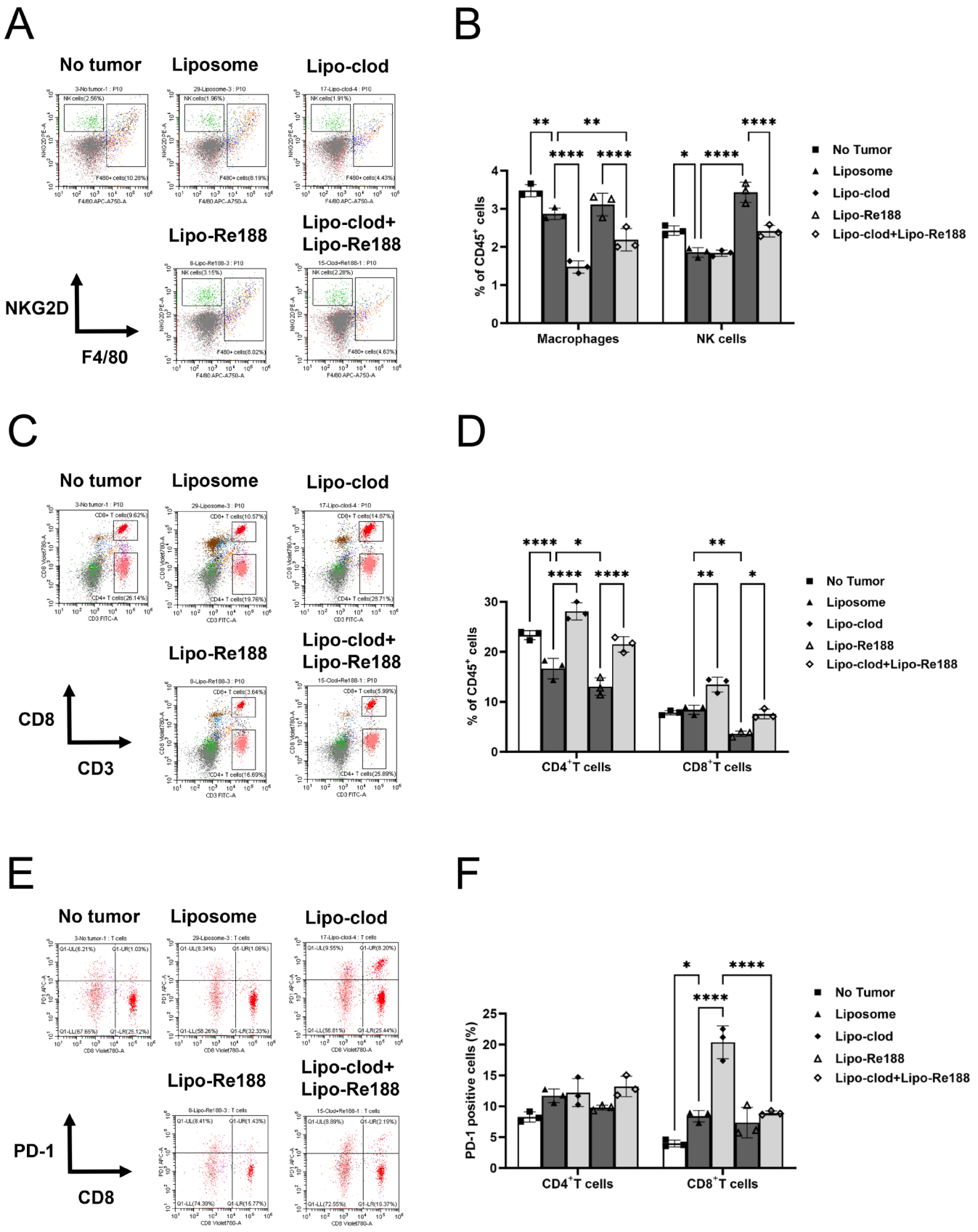

FIGURE 2 | Immunomodulatory effects of Lipo-Re188 in the spleen following macrophage depletion. Representative flow cytometry plots of splenic macrophages and NK cells (A) identified by F4/80 and NKG2D expression and quantification data (B) ($n = 3$). Representative flow cytometry plots of splenic $CD4^+$ and $CD8^+$ T cells (C) identified by CD3 and CD8 expression and quantification data (D) ($n = 3$). (E) Representative flow cytometry plots of exhausted T cells (CD8 vs. PD-1). (F) Frequency of PD-1^+ cells among $CD4^+$ and $CD8^+$ T cells ($n = 3$). (G) Representative flow cytometry plots of inflammatory cytokine plots on day 4 post-treatment. Plasma concentrations of IL-1α (H) and GM-CSF (I) across treatment groups ($n = 3$). All data are shown as mean ± SD. Statistical analysis was performed using one-way ANOVA with Tukey's post hoc test. *$p < 0.05$; **$p < 0.01$; ***$p < 0.001$; ****$p < 0.0001$.

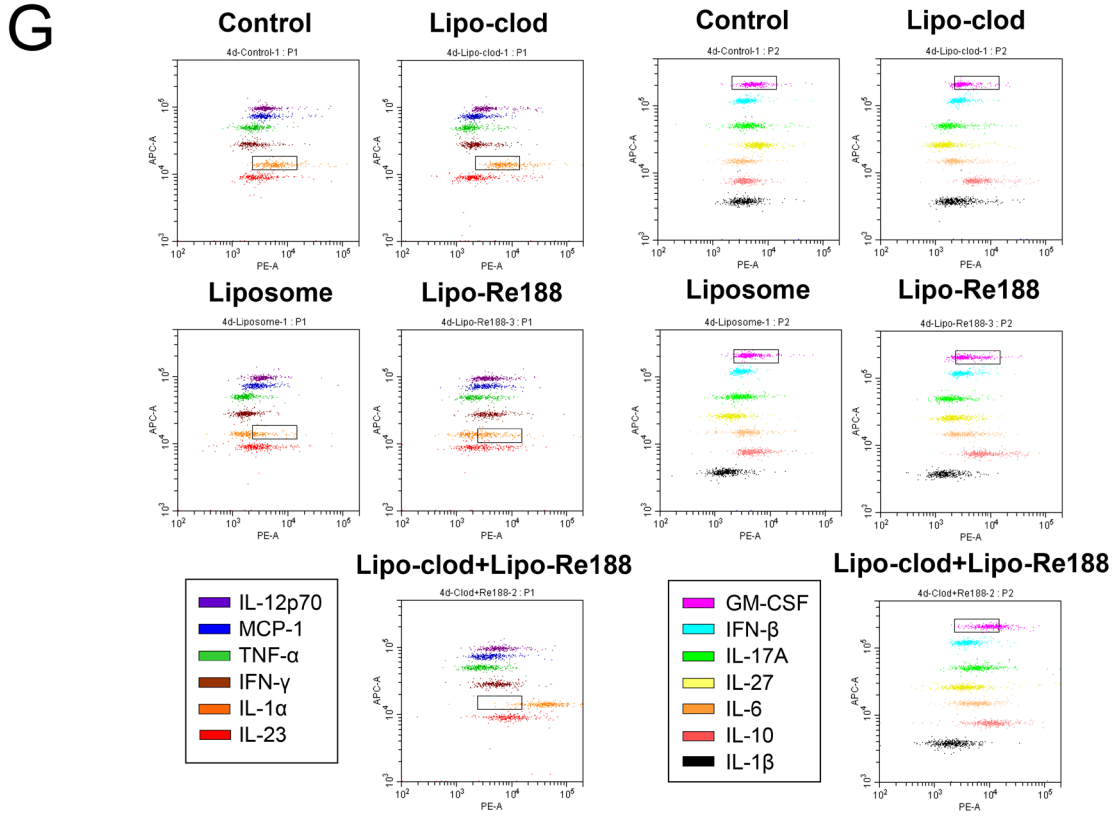

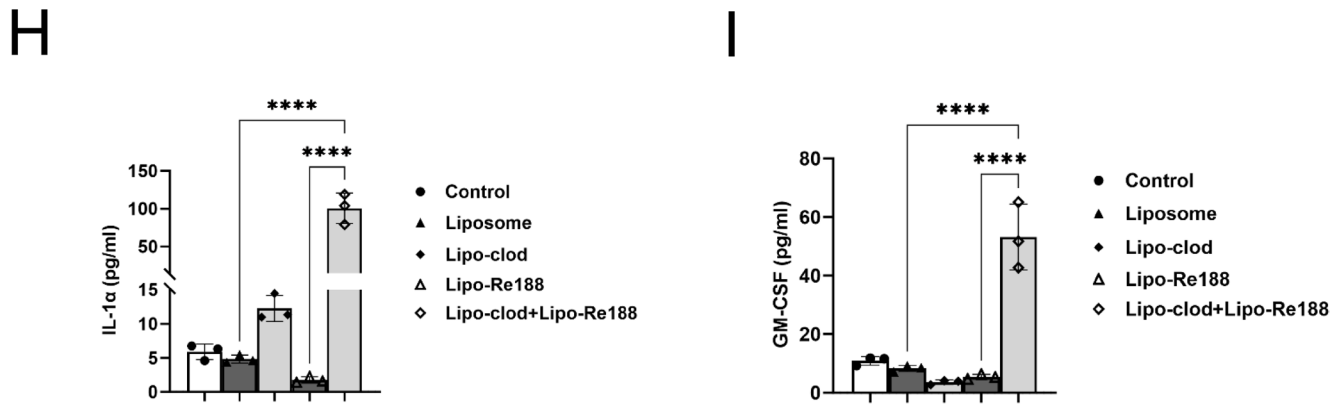

FIGURE 2 | (Continued)

was administered to the Lipo-Re188 and combination groups. Intravenous administration of Lipo-clod effectively suppresses macrophages within 2 days [47], which represents the optimal window for combination therapy. Therefore, Lipo-clod was administered intravenously 2 days prior to Lipo-Re188 (Figure 1A). IVIS analysis revealed that prior depletion of macrophages significantly enhanced the tumor-suppressive effect of Lipo-Re188 compared to the liposome control group (Figure 1B,C). Median survival was extended from 21 days in the liposome group to 31 days with Lipo-Re188 monotherapy and further to 37 days with combination therapy (Figure 1D). Regarding systemic toxicity, body weight, white blood cell (WBC) counts, and indicators of liver (alanine aminotransferase, ALT) and kidney function (creatinine, CRE) were monitored. No significant changes in body weight were observed across groups (Figure 1E). Both Lipo-clod and Lipo-Re188 treatments transiently reduced WBC counts on days 5 and 10 post-treatment, which recovered by day 15 (Figure 1F). A mild elevation in ALT was detected in 20% of the control mice on day 15, while combination therapy did not significantly alter ALT levels compared to the control (Figure 1G). CRE levels remained within the normal range in all groups (Figure 1H). Collectively, these results indicate that macrophage depletion significantly enhances the antitumor effect of Lipo-Re188 without causing notable systemic toxicity.

3.2 | Macrophage Depletion Increases Tumor Accumulation of Lipo-Re188

To evaluate the effect of macrophage depletion on the biodistribution of Lipo-Re188, tissue radioactivity was measured at multiple time points in CT26-luc-bearing mice (Table 1).

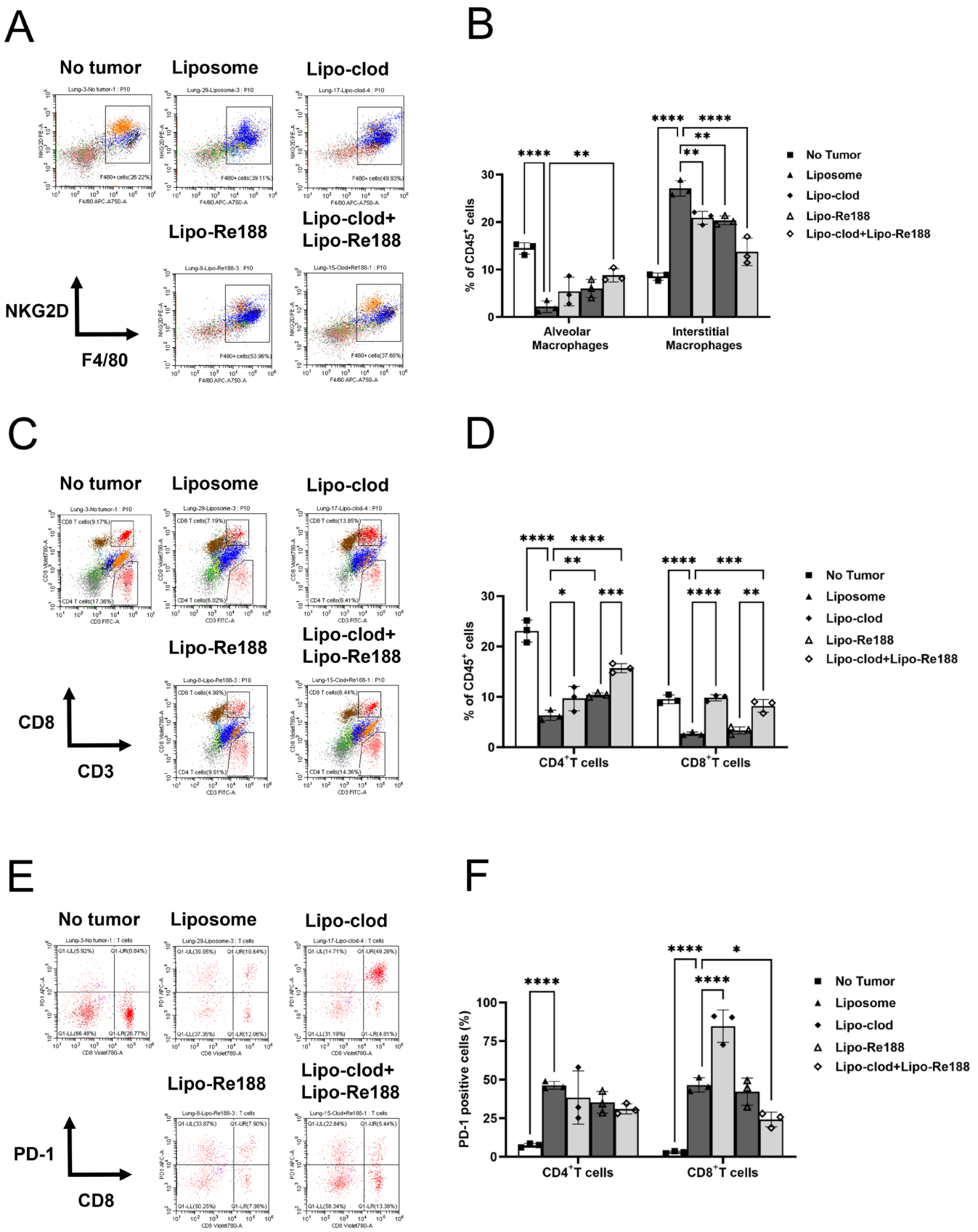

FIGURE 3 | Legend on next page.

At 1 h post-injection, Lipo-Re188 was primarily detected in the blood (23.29% ± 2.72% injected dose per gram, ID/g). Macrophage depletion significantly increased circulating levels (38.37% ± 13.22% ID/g). Notably, Lipo-clod pretreatment resulted in a 4-fold increase in splenic accumulation (34.61% ± 12.54% vs. 8.06% ± 0.61%). At 24 h, Lipo-Re188 was predominantly

FIGURE 3 | Lipo-Re188 reshapes the tumor immune microenvironment following macrophage depletion. (A) Representative flow cytometry plots identifying alveolar and interstitial macrophages in the tumor microenvironment (TME), based on F4/80 and NKG2D expression. (B) Quantification of macrophage subsets in the TME among CD45$^+$ cells ($n = 3$). (C) Representative flow cytometry plots of CD4$^+$ and CD8$^+$ T cells (CD3 vs. CD8) in the TME. (D) Quantification of T cell subsets in the TME ($n = 3$). (E) Representative plots of PD-1$^+$ exhausted CD4$^+$ and CD8$^+$ T cells (CD8 vs. PD-1). (F) Proportion of PD-1$^+$ cells among CD4$^+$ and CD8$^+$ T cells in the TME ($n = 3$). Data are shown as mean ± SD. Statistical significance was determined by one-way ANOVA with Tukey's post hoc test. *$p < 0.05$; **$p < 0.01$; ***$p < 0.001$; ****$p < 0.0001$.

distributed in the blood, liver, and spleen. Combination therapy elevated splenic uptake (28.78% ± 7.48% vs. 12.20% ± 1.99%) and reduced hepatic accumulation (4.29% ± 1.11% vs. 11.45% ± 3.70%). This trend persisted at 48 h, with significantly increased retention in the spleen, decreased liver uptake, and higher blood levels in the combination group compared to Lipo-Re188 alone. Importantly, macrophage depletion significantly increased Lipo-Re188 levels in the lungs (5.11% ± 1.03% vs. 2.36% ± 0.46%), and the tumor-to-muscle uptake ratio improved from 13.89 to 23.22. These data suggest that macrophage elimination prolongs the systemic circulation of Lipo-Re188, enhances tumor targeting, and reduces hepatic sequestration, as well as improves both therapeutic efficacy and hepatic toxicity.

3.3 | Lipo-Re188 Modulates Splenic Immune Profile Following Macrophage Depletion

To evaluate the impact of macrophage depletion and Lipo-Re188 treatment on systemic immunity, we analyzed immune cell populations in the spleen across five experimental groups—no tumor, liposome, Lipo-clod, Lipo-Re188, and Lipo-clod + Lipo-Re188—using multicolor flow cytometry. Normal mice (no tumor group) served as a negative control to assess tumor-associated alterations in immune profiles. A total of ten immune cell subsets were examined with clearly separated gating: polymorphonuclear myeloid-derived suppressor cells (PMN-MDSC), monocytic MDSC (M-MDSC), macrophages, dendritic cells, eosinophils, natural killer (NK) cells, B cells, natural killer T (NKT) cells, CD4$^+$ T cells, and CD8$^+$ T cells. Gating strategies for each population are detailed in the Materials and Methods section. Treatment with Lipo-clod effectively depleted splenic macrophages and led to a significant induction of both CD4$^+$ and CD8$^+$ T cells on day 16 post-treatment (Figure 2A–D). Although macrophage depletion increased the proportion of CD8$^+$ T cells compared to the liposome group, a significant fraction of these cells expressed PD-1, indicative of an exhausted phenotype (Figure 2E,F). In contrast, PD-1 expression was not upregulated in CD4$^+$ T cells following Lipo-clod treatment, suggesting these cells retained functionality. Lipo-Re188 monotherapy significantly increased NK and B cell populations but concurrently reduced CD4$^+$ and CD8$^+$ T cell numbers compared to the liposome group (Figure 2A–D; Figure S1A). Notably, combination treatment (Lipo-clod + Lipo-Re188) led to further reductions in macrophages and NK cells while rescuing CD4$^+$ and CD8$^+$ T cell populations relative to Lipo-Re188 alone (Figure 2A–D). Exhausted CD8$^+$ T cells (PD-1$^+$) were significantly reduced in the combination group, suggesting improved T cell functionality (Figure 2E,F). While Lipo-clod diminished the Lipo-Re188-induced increase in NK cells, B cell levels remained elevated following combination treatment, even exceeding those in normal mice (Figure S1A). Additionally, both PMN-MDSC and M-MDSC populations were significantly suppressed by the combination therapy on day 16 post-treatment (Figure S1B).

We further assessed circulating inflammatory cytokines on day 4 post-treatment and found that IL-1α and GM-CSF levels were significantly elevated in the combination group compared to either the liposome or Lipo-Re188 groups (Figure 2G–I). These findings suggest that Lipo-clod + Lipo-Re188 therapy enhances systemic antitumor immunity accompanied by elevating B cells, reducing MDSC-mediated immunosuppression, restoring T cell function, and promoting pro-inflammatory cytokine responses.

3.4 | Lipo-Re188 Reprograms Tumor Microenvironment Following Macrophage Depletion

Tumor microenvironment (TME) is a critical determinant of treatment efficacy. To further characterize local immune modulation, we analyzed immune cell subsets in the TME using flow cytometry. Ten immune cell types in the TME were quantified: PMN-MDSC, M-MDSC, alveolar macrophages, interstitial macrophages, eosinophils, NK cells, B cells, NKT cells, CD4$^+$ T cells, and CD8$^+$ T cells. Lipo-clod treatment effectively reduced interstitial macrophages and NK cells, while having minimal impact on alveolar macrophages (Figure 3A,B). Although both CD4$^+$ and CD8$^+$ T cells were elevated post-Lipo-clod, CD8$^+$ T cells exhibited high PD-1 expression, indicative of exhaustion. Lipo-Re188 monotherapy led to further decreases in CD8$^+$ T cells, without notable increases in NK and B cells within the TME by day 16 (Figure 3C,D; Figure S1C,E). Importantly, combination therapy significantly increased intratumoral CD4$^+$ T cells, CD8$^+$ T cells, and B cells compared to Lipo-Re188 alone (Figure 3C,D; Figure S1C). PD-1$^+$ CD8$^+$ T cells were lowest in the combination group, indicating restoration of cytotoxic T cell activity (Figure 3E,F). Additionally, interstitial macrophages, PMN-MDSC, and M-MDSC were significantly suppressed following combination treatment. Together, these results suggest that co-administration of Lipo-clod and Lipo-Re188 reprograms the TME by enhancing functional CD4$^+$ and CD8$^+$ T cell infiltration, promoting B cell recruitment, and reducing immunosuppressive MDSC and macrophage populations. These coordinated immune changes in the TME can serve as biomarkers correlated with therapeutic efficacy against lung metastases.

3.5 | PD-L1 Blockage Enhances Therapeutic Efficacy of Lipo-Re188 After Macrophage Depletion

Our previous work demonstrated that PD-L1 blockade provides more sustained suppression of PD-1 expression than direct PD-1 inhibition in the lung metastasis mouse model [48]. In addition,

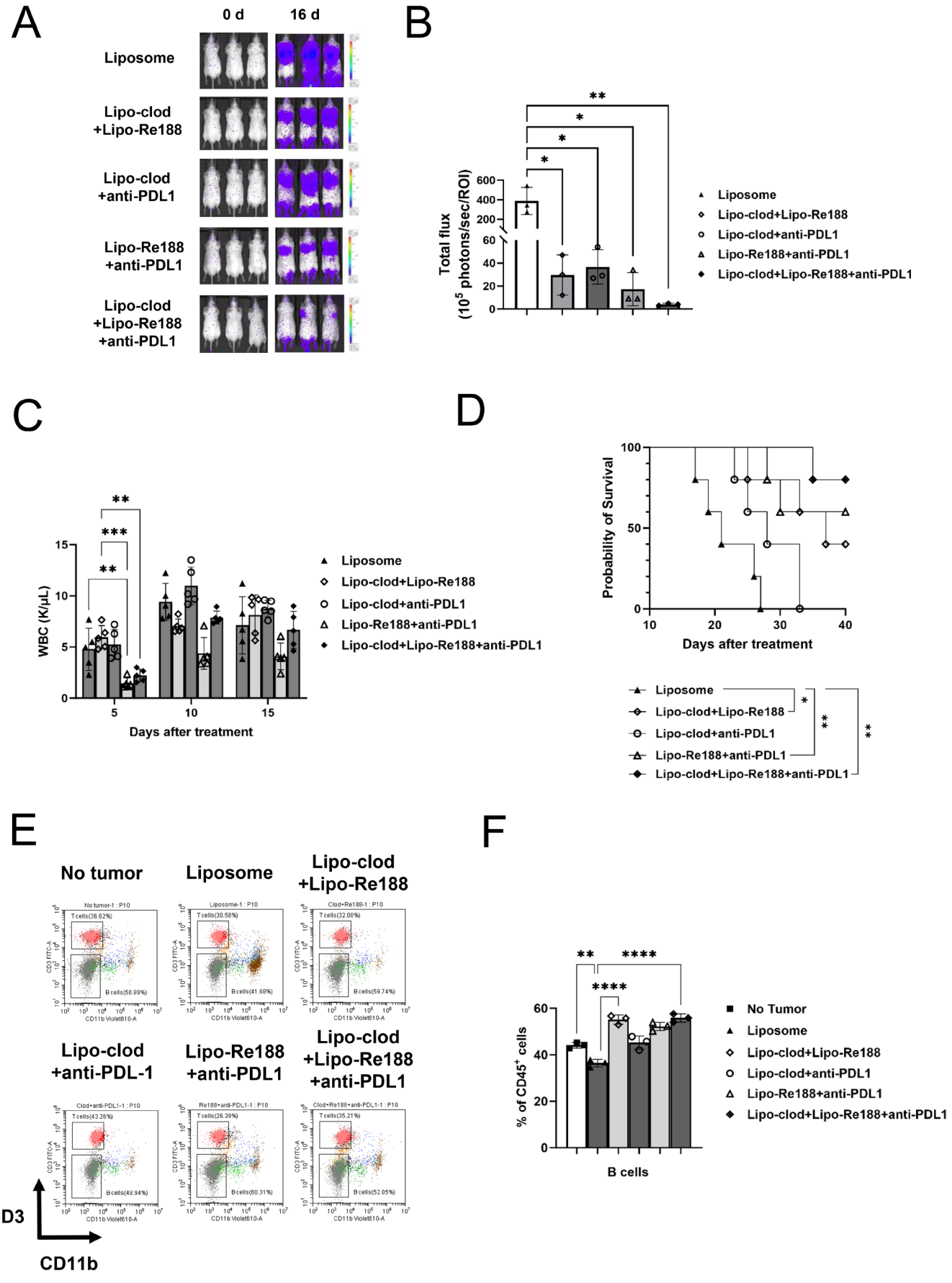

FIGURE 4 | PD-L1 blockade synergizes with Lipo-Re188 to improve therapeutic efficacy following macrophage depletion. (A) CT26-luc lung metastasis-bearing mice were randomized into five treatment groups: Liposome, Lipo-clod+Lipo-Re188, Lipo-clod+anti–PD-L1, Lipo-Re188 + anti–PD-L1, and Lipo-clod+Lipo-Re188 + anti–PD-L1. IVIS images of lung metastases were shown on days 0 and 16 post-treatment ($n = 3$). (B) Quantification of lung tumor burden based on total photon flux within the lung ROI on days 16 post-treatment ($n = 3$). (C) White blood cell counts monitored over 15 days post-treatment ($n = 5$). (D) Kaplan–Meier survival curves of each group ($n = 5$). (E) Representative flow cytometry plots of splenic B cells (CD11b vs. CD3) across six groups, including normal mice no tumor group. (F) Quantification of B cells among splenic $CD45^+$ cells ($n = 3$). (G) Representative flow cytometry plots of B cells in the TME (CD11b vs. CD3). (H) Quantification of B cells in the TME among $CD45^+$ cells ($n = 3$). (I) Quantification of alveolar and interstitial macrophages in the TME ($n = 3$). Data are presented as mean ± SD. Statistical analyses were conducted using one-way ANOVA with Tukey's multiple comparisons test or log-rank test for survival. $^*p < 0.05$; $^{**}p < 0.01$; $^{***}p < 0.001$; $^{****}p < 0.0001$.

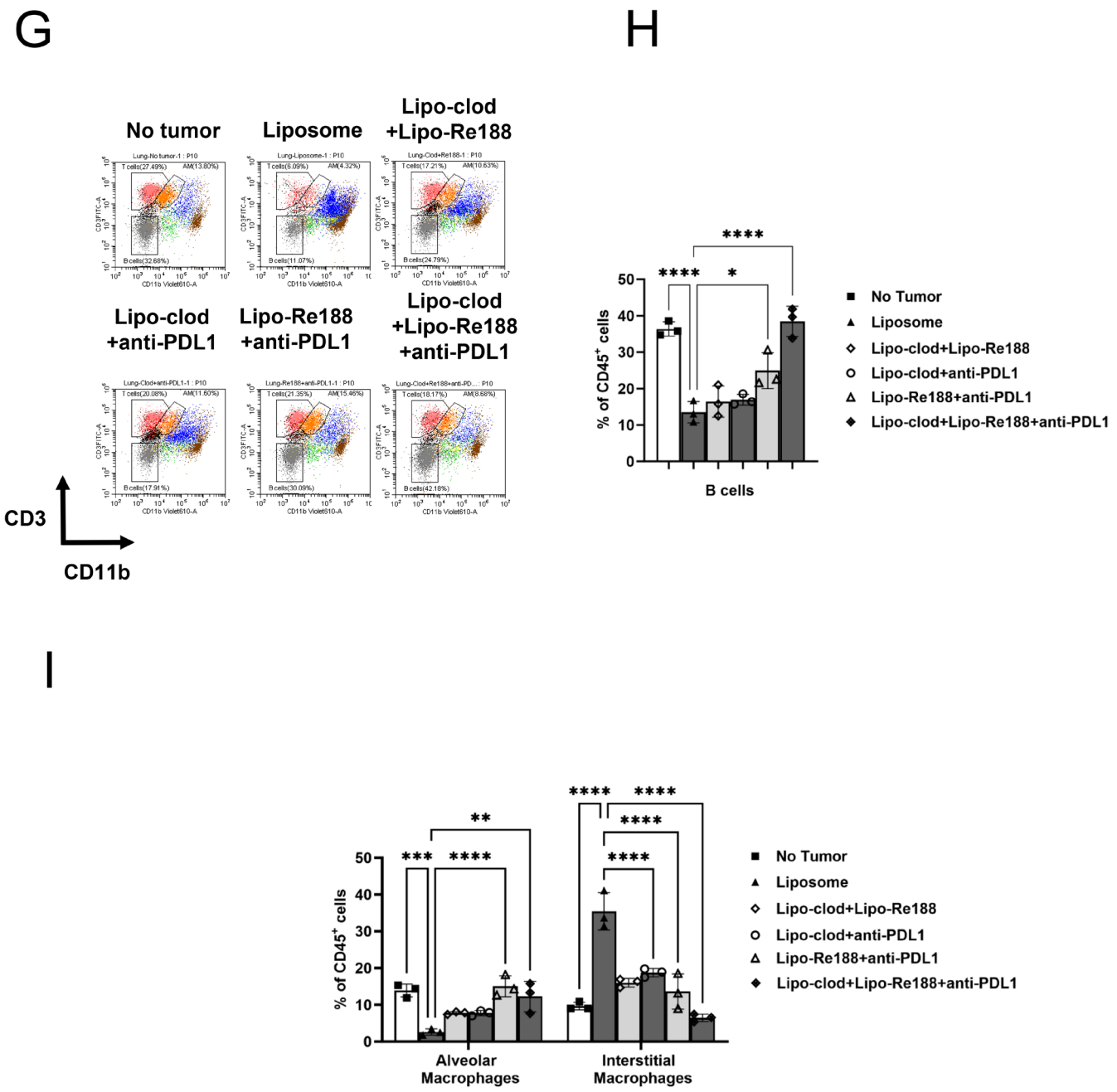

FIGURE 4 | (Continued)

Lipo-Re188 treatment significantly upregulated PD-L1 expression at early time points (Figure S2), suggesting a potential immune evasion mechanism. Based on these findings, we selected PD-L1 blockade as a combinatorial strategy to enhance tumor control against lung metastases. After assessing by IVIS imaging, and mice were randomly assigned to six groups: no tumor, liposome, Lipo-clod+Lipo-Re188, Lipo-clod+anti-PD-L1, Lipo-Re188 + anti-PD-L1, and Lipo-clod+Lipo-Re188 + anti-PD-L1. Lipo-clod was

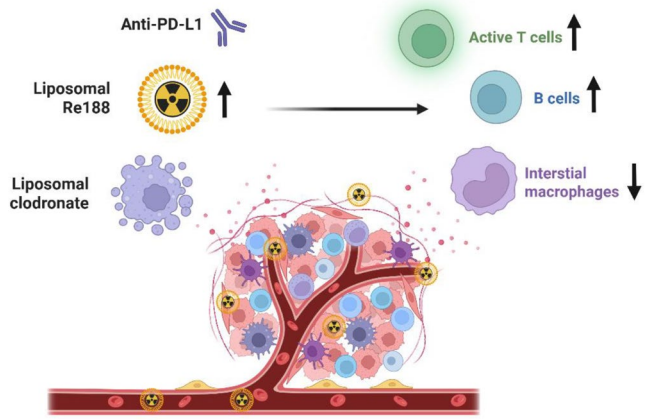

FIGURE 5 | PD-L1 blockade potentiates the anti-tumor activity of Lipo-Re188 following macrophage depletion. Liposomal clodronate (Lipo-clod) depletes macrophages and monocytes, leading to increased T cell infiltration, while Lipo-Re188 reduces T cell levels but promotes B cell expansion at later stages. The combination of Lipo-clod, Lipo-Re188, and anti-PD-L1 therapy preserves the Lipo-Re188-induced B cell population and mitigates immunosuppressive barriers associated with monocyte-derived macrophages and PD-L1 expression. This triple therapy enhances functional T cell and B cell responses within the TME and improves therapeutic outcomes against lung metastases. Created with BioRender.com.

administered intravenously 2 days prior to Lipo-Re188 injection (day 0), while anti-PD-L1 antibody (7.5 mg/kg) was administered intraperitoneally on days 0, 2, and 4 post-Lipo-Re188 injection. IVIS analysis revealed that the triple combination of Lipo-clod, Lipo-Re188, and anti-PD-L1 achieved the most pronounced inhibition of lung tumor growth (Figure 4A,B). Myelosuppression was observed on day 5 following combined treatment with Lipo-Re188, Lipo-clod, and anti-PD-L1, with hematologic recovery by days 10 and 15 (Figure 4C). No difference in body weight was noted among groups, indicating a lack of significant systemic toxicity (data not shown). Survival analysis further confirmed that the triple therapy significantly extended median survival compared to liposome groups (Figure 4D). To evaluate the possible underlying immune mechanisms, we analyzed immune cell populations in the spleen and TME. Consistent with previous findings, the combination of Lipo-clod and Lipo-Re188 significantly increased splenic B cell levels, an effect also observed in the Lipo-Re188 + anti-PD-L1 and Lipo-clod+Lipo-Re188 + anti-PD-L1 groups (Figure 4E,F). Within the TME, triple therapy led to a marked elevation of B cells—exceeding levels observed in normal mice—and was associated with enhanced therapeutic efficacy (Figure 4G,H). Interstitial macrophages, which arise from M-MDSC and contribute to immunosuppression, were markedly reduced in the triple treatment group compared to liposome controls (Figure 4I), highlighting their potential as a biomarker for therapeutic response. Although Lipo-clod alone or in combination (double or triple regimens) increased T cell levels in both the spleen and TME, these changes did not strongly correlate with the therapeutic efficacy of triple combination treatment (Figure S3A,C). In summary, prior depletion of macrophages not only enhanced Lipo-Re188 accumulation within the TME but also promoted the recruitment of B cells and reduced interstitial macrophages. Importantly, the feedback upregulation of PD-L1 following Lipo-clod/Lipo-Re188 was effectively counteracted by PD-L1 blockade, thereby remodeling the TME into a more immunostimulatory and tumor-suppressive environment.

4 | Discussion

Rhenium-188 (Re188) is a promising theranostic radionuclide due to its high-energy β-emission, moderate physical half-life, and cost-efficient generator-based production. Encapsulation of Re-188 in liposomes (Lipo-Re188) significantly prolongs systemic circulation and facilitates preferential accumulation in tumors via the EPR effect [49]. However, hepatic clearance of Lipo-Re188 by the mononuclear phagocyte system (MPS), particularly Kupffer cells in the liver, can result in hepatotoxicity and limit therapeutic efficacy. In this study, we demonstrated that prior depletion of macrophages using liposomal clodronate (Lipo-clod) enhanced the accumulation of Lipo-Re188 in tumor tissues and peripheral blood, thereby improving tumor growth suppression in a lung metastasis model. The combination of Lipo-clod and Lipo-Re188 altered the biodistribution profile, increasing splenic accumulation three-fold and reducing hepatic accumulation by half. Although increased accumulation of Lipo-Re188 was observed in the spleen and bone marrow following macrophage depletion, this did not result in sustained immunosuppression. Immune cell populations within these hematopoietic organs exhibited the capacity for repopulation at later time points, suggesting that the transient exposure to Lipo-Re188 was not sufficient to induce irreversible damage. Unlike the spleen and bone marrow, the regenerative response of hepatic immune and parenchymal cells may be slower or incomplete following repeated radionuclide exposure. These findings indicate that the immune system retains regenerative potential following low-dose Lipo-Re188 treatment, thereby supporting the safety profile of this therapeutic approach when combined with macrophage depletion.

The MPS is a dynamic and self-regulating network that orchestrates the clearance of pathogens, apoptotic cells, and exogenous particles such as nanoparticles and liposomes [50, 51]. Upon Kupffer cell depletion, compensatory mechanisms are initiated, including increased output of monocyte-derived suppressor cells (M-MDSC) from the bone marrow to preserve systemic phagocytic function. Additionally, we observed Lipo-clod reduced not only macrophages but also M-MDSC, NK cells, dendritic cells, and B cells (Figure S2E,F), suggesting broader immunomodulatory effects. Emerging data indicate Lipo-clod is also internalized by neutrophils, potentially contributing to its anti-inflammatory activity in vivo [52]. Notably, Campbell et al. reported that repeated intradermal injections of Lipo-clod restored $CD8^+$ T cell numbers in a psoriasiform mouse model [53]. In our study, Lipo-clod significantly increased both $CD4^+$ and $CD8^+$ T cell populations post-treatment. Further characterization is needed to determine whether these $CD4^+$ T cells include regulatory T cell subsets. Lipo-Re188 monotherapy consistently increased NK and B cell populations in both the spleen and TME. The combination therapy led to sustained elevation of intratumoral B cells and effectively restored T cell populations previously suppressed by Lipo-Re188. These observations support the notion that Lipo-clod augments the antitumor activity of

Lipo-Re188 by reshaping the immune landscape, notably increasing functional T and B cells in the TME. Prior studies on other β- and γ-emitting radionuclides (^{90}Y, ^{131}I, and ^{177}Lu) also demonstrated immune-modulating properties. For instance, Vito et al. found that intratumoral ^{177}Lu-BSA-tetrazine reduced CD4$^+$ and CD8$^+$ T cell infiltration in EO771 tumors [54], while systemic administration of ^{90}Y-NM600 increased CD8$^+$ T cell infiltration but upregulated immune checkpoint markers in prostate cancer models [55]. Hernandez et al. reported enhanced CD8$^+$ T cell infiltration and decreased FOXP3$^+$ cells following ^{90}Y-NM600 in T-cell lymphoma [56], and Patel et al. observed NK cell enrichment in B78 melanoma tumors post ^{90}Y-NM600 therapy [29]. Similarly, ^{177}Lu-DOTATATE enhanced NK cell infiltration with FasL expression in neuroendocrine tumor models [57]. Our findings further illustrate the capacity of radionuclide therapy to modulate systemic and local immune responses. Notably, Lipo-Re188 monotherapy increased NK cells, CD4$^+$ T cell, and B cell infiltration in the TME. Given the dualistic role of B cells in cancer [58–60], our data identifying increased systemic and intratumoral B cells following Lipo-Re188 treatment suggest a potentially beneficial immunomodulatory role. However, whether these B cells represent immunosuppressive regulatory B cells (Bregs) or tumor-suppressive effector B cells remains unclear. Functional characterization, such as profiling their cytokine production, will be an important direction for future research to clarify the precise contribution of B cell subsets to the therapeutic outcome.

Radionuclide therapies can modulate cytokine responses. Prior studies showed ^{177}Lu-DOTA-2P(FAPI)$_2$ with anti-PD-L1 activated IL-1α, ^{90}Y-resin microspheres correlated with IL-1β in HCC, and ^{177}Lu-conjugated antibodies increased IL-10, IFN, and TGFβ [61–63]. In our study, Lipo-Re188 plus Lipo-clod elevated IL-1α and GM-CSF levels. IL-1α is a pro-inflammatory cytokine that induces GM-CSF and helps protect against radiation-induced hematopoietic injury. GM-CSF can boost antitumor immunity but may also promote MDSC expansion, showing both beneficial and suppressive roles in the immune response [64, 65]. These findings highlight the complex inflammatory cascades triggered by radiopharmaceutical therapy.

Radiopharmaceutical monotherapy often fails to induce durable tumor regression, and combinatorial strategies with immune checkpoint inhibitors (ICI) have shown synergistic potential [66, 67]. Thus, therapy-induced immunosuppression is a critical barrier to sustained response. In our study, Lipo-clod enhanced CD4$^+$ and CD8$^+$ T cells but was associated with elevated PD-1 expression on CD8$^+$ T cells (Figure 2E,F). Moreover, Lipo-Re188 treatment induced compensatory increases in Ly6G$^+$ cells and PD-L1 expression (Figure S2). These findings rationalize the use of triple combination therapy with Lipo-clod, Lipo-Re188, and anti-PD-L1, which reshapes the tumor microenvironment, enhances functional T and B cells, and potentially mitigates off-target toxicity associated with radionuclide accumulation (Figure 5). A limitation is that long-term immune memory was not assessed, and whether surviving mice resist cancer cells rechallenge remains to be determined. Our concept of combining Lipo-clod with Lipo-Re188 and anti-PD-L1 could be extended to the clinic by substituting FDA-approved macrophage-targeting agents such as the CSF1R inhibitor pexidartinib or trabectedin [68, 69]. This strategy highlights the translational potential of macrophage modulation to enhance radiopharmaceutical–immunotherapy combinations.

Our study underscores the immunological and therapeutic effects of liposome-encapsulated β-emitter Lipo-Re188 in a lung metastasis model. These insights are instrumental for developing rational combinations of radiopharmaceuticals with immunotherapies such as ICI to optimize clinical outcomes.

Author Contributions

Shin-Yi Liu: conceptualization, data curation, formal analysis, investigation, methodology, validation, visualization, writing – original draft. **Liang-Ting Lin:** investigation, methodology, resources. **Chih-Hsien Chang:** funding acquisition, resources, supervision. **Yu-Jen Chen:** conceptualization, funding acquisition, project administration, resources, supervision, writing – review and editing.

Ethics Statement

Animal experimental procedures were approved by the Institutional Animal Care and Use Committee (MMH-A-S-108-25) of Mackay Memorial Hospital.

Conflicts of Interest

The authors declare no conflicts of interest.

References

1. G. Sgouros, L. Bodei, M. R. McDevitt, and J. R. Nedrow, "Radiopharmaceutical Therapy in Cancer: Clinical Advances and Challenges," *Nature Reviews. Drug Discovery* 19 (2020): 589–608, https://doi.org/10.1038/s41573-020-0073-9.

2. L. Bodei, K. Herrmann, H. Schöder, A. M. Scott, and J. S. Lewis, "Radiotheranostics in Oncology: Current Challenges and Emerging Opportunities," *Nature Reviews. Clinical Oncology* 19 (2022): 534–550, https://doi.org/10.1038/s41571-022-00652-y.

3. D. Guimarães, A. Cavaco-Paulo, and E. Nogueira, "Design of Liposomes as Drug Delivery System for Therapeutic Applications," *International Journal of Pharmaceutics* 601 (2021): 120571, https://doi.org/10.1016/j.ijpharm.2021.120571.

4. S. Zhou, Y. Luo, and J. F. Lovell, "Vaccine Approaches for Antigen Capture by Liposomes," *Expert Review of Vaccines* 22 (2023): 1022–1040, https://doi.org/10.1080/14760584.2023.2274479.

5. N. Zhang, M. Li, Z. Hou, et al., "From Vaccines to Nanovaccines: A Promising Strategy to Revolutionize Rheumatoid Arthritis Treatment," *Journal of Controlled Release* 350 (2022): 107–121, https://doi.org/10.1016/j.jconrel.2022.08.020.

6. H. R. Kim, H. B. Cho, S. Lee, J. I. Park, H. J. Kim, and K. H. Park, "Fusogenic Liposomes Encapsulating Mitochondria as a Promising Delivery System for Osteoarthritis Therapy," *Biomaterials* 302 (2023): 122350, https://doi.org/10.1016/j.biomaterials.2023.122350.

7. Y. Xie, Z. Ren, H. Chen, et al., "A Novel Estrogen-Targeted PEGylated Liposome Co-Delivery Oxaliplatin and Paclitaxel for the Treatment of Ovarian Cancer," *Biomedicine & Pharmacotherapy* 160 (2023): 114304, https://doi.org/10.1016/j.biopha.2023.114304.

8. M. Kim, J. S. Lee, W. Kim, et al., "Aptamer-Conjugated Nano-Liposome for Immunogenic Chemotherapy With Reversal of Immunosuppression," *Journal of Controlled Release* 348 (2022): 893–910, https://doi.org/10.1016/j.jconrel.2022.06.039.

9. Y. Zong, Y. Lin, T. Wei, and Q. Cheng, "Lipid Nanoparticle (LNP) Enables mRNA Delivery for Cancer Therapy," *Advanced Materials* 35 (2023): e2303261, https://doi.org/10.1002/adma.202303261.

10. A. Shinto, "Rhenium 188: The Poor Man's Yttrium," *World Journal of Nuclear Medicine* 16 (2017): 1–2, https://doi.org/10.4103/1450-1147.198225.

11. A. Dash, F. F. Knapp, and M. R. Pillai, "Targeted Radionuclide Therapy—An Overview," *Current Radiopharmaceuticals* 6 (2013): 152–180.

12. L. Uccelli, P. Martini, L. Urso, et al., "Rhenium Radioisotopes for Medicine, a Focus on Production and Applications," *Molecules* 27 (2022): 5283, https://doi.org/10.3390/molecules27165283.

13. C. M. Chang, K. L. Lan, W. S. Huang, et al., "(188)re-Liposome Can Induce Mitochondrial Autophagy and Reverse Drug Resistance for Ovarian Cancer: From Bench Evidence to Preliminary Clinical Proof-Of-Concept," *International Journal of Molecular Sciences* 18 (2017): 903, https://doi.org/10.3390/ijms18050903.

14. L. T. Lin, C. H. Chang, H. L. Yu, et al., "Evaluation of the Therapeutic and Diagnostic Effects of PEGylated Liposome-Embedded 188Re on Human Non-Small Cell Lung Cancer Using an Orthotopic Small-Animal Model," *Journal of Nuclear Medicine* 55 (2014): 1864–1870, https://doi.org/10.2967/jnumed.114.140418.

15. W. H. Hsu, S. Y. Liu, Y. J. Chang, C. H. Chang, G. Ting, and T. W. Lee, "The PEGylated Liposomal Doxorubicin Improves the Delivery and Therapeutic Efficiency of 188Re-Liposome by Modulating Phagocytosis in C26 Murine Colon Carcinoma Tumor Model," *Nuclear Medicine and Biology* 41 (2014): 765–771, https://doi.org/10.1016/j.nucmedbio.2014.05.142.

16. Y. J. Chang, C. Y. Yu, C. W. Hsu, et al., "Molecular Imaging and Therapeutic Efficacy of 188Re-(DXR)-Liposome-BBN in AR42J Pancreatic Tumor-Bearing Mice," *Oncology Reports* 28 (2012): 1736–1742, https://doi.org/10.3892/or.2012.1978.

17. C. H. Chang, S. Y. Liu, C. W. Chi, et al., "External Beam Radiotherapy Synergizes ^{188}re-Liposome Against Human Esophageal Cancer Xenograft and Modulates ^{188}re-Liposome Pharmacokinetics," *International Journal of Nanomedicine* 10 (2015): 3641–3649, https://doi.org/10.2147/IJN.S80302.

18. C. Y. Chang, C. C. Chen, L. T. Lin, et al., "PEGylated Liposome-Encapsulated Rhenium-188 Radiopharmaceutical Inhibits Proliferation and Epithelial–Mesenchymal Transition of Human Head and Neck Cancer Cells In Vivo With Repeated Therapy," *Cell Death Discovery* 4 (2018): 100, https://doi.org/10.1038/s41420-018-0116-8.

19. M. Hashida, "Advocation and Advancements of EPR Effect Theory in Drug Delivery Science: A Commentary," *Journal of Controlled Release* 346 (2022): 355–357, https://doi.org/10.1016/j.jconrel.2022.04.031.

20. S. Asadian, H. Mirzaei, B. A. Kalantari, et al., "β-Radiating Radionuclides in Cancer Treatment, Novel Insight Into Promising Approach," *Pharmacological Research* 160 (2020): 105070, https://doi.org/10.1016/j.phrs.2020.105070.

21. S. J. Wang, W. S. Huang, C. M. Chuang, et al., "A Phase 0 Study of the Pharmacokinetics, Biodistribution, and Dosimetry of 188Re-Liposome in Patients With Metastatic Tumors," *EJNMMI Research* 9 (2019): 46, https://doi.org/10.1186/s13550-019-0509-6.

22. K. Liepe, J. J. Zaknun, A. Padhy, et al., "Radiosynovectomy Using Yttrium-90, Phosphorus-32 or Rhenium-188 Radiocolloids Versus Corticoid Instillation for Rheumatoid Arthritis of the Knee," *Annals of Nuclear Medicine* 25 (2011): 317–323, https://doi.org/10.1007/s12149-011-0467-1.

23. E. Garin, H. Rakotonirina, F. Lejeune, et al., "Effect of a 188 re-SSS Lipiodol/131I-Lipiodol Mixture, 188 re-SSS Lipiodol Alone or 131I-Lipiodol Alone on the Survival of Rats With Hepatocellular Carcinoma," *Nuclear Medicine Communications* 27 (2006): 363–369, https://doi.org/10.1097/00006231-200604000-00008.

24. N. Lepareur, B. Ramée, M. Mougin-Degraef, and M. Bourgeois, "Clinical Advances and Perspectives in Targeted Radionuclide Therapy," *Pharmaceutics* 15 (2023): 1733, https://doi.org/10.3390/pharmaceutics15061733.

25. C. A. Ferreira, H. K. Potluri, M. Mahmoudian, et al., "Immunomodulatory Effects of Alpha vs Beta Radiopharmaceutical Therapy in Murine Prostate Cancer," *Frontiers in Immunology* 16 (2025): 1563387, https://doi.org/10.3389/fimmu.2025.1563387.

26. Q. Sun, J. Li, Z. Ding, and Z. Liu, "Radiopharmaceuticals Heat Anti-Tumor Immunity," *Theranostics* 13 (2023): 767–786, https://doi.org/10.7150/thno.79806.

27. J. Constanzo, A. Parach, T. David, et al., "MHC-I–Driven Antitumor Immunity Counterbalances Low Absorbed Doses of Radiopharmaceutical Therapy," *Journal of Nuclear Medicine* 66 (2025): 785–792, https://doi.org/10.2967/jnumed.124.268857.

28. J. C. Jagodinsky, W. J. Jin, A. M. Bates, et al., "Temporal Analysis of Type 1 Interferon Activation in Tumor Cells Following External Beam Radiotherapy or Targeted Radionuclide Therapy," *Theranostics* 11 (2021): 6120–6137, https://doi.org/10.7150/thno.54881.

29. R. B. Patel, R. Hernandez, P. Carlson, et al., "Low-Dose Targeted Radionuclide Therapy Renders Immunologically Cold Tumors Responsive to Immune Checkpoint Blockade," *Science Translational Medicine* 13 (2021): eabb3631, https://doi.org/10.1126/scitranslmed.abb3631.

30. C. J. Maks, X. S. Wan, J. H. Ware, et al., "Analysis of White Blood Cell Counts in Mice After Gamma- or Proton-Radiation Exposure," *Radiation Research* 176 (2011): 170–176, https://doi.org/10.1667/RR2413.1.

31. A. Muralidhar, R. Hernandez, Z. S. Morris, et al., "Myeloid-Derived Suppressor Cells Attenuate the Antitumor Efficacy of Radiopharmaceutical Therapy Using 90Y-NM600 in Combination With Androgen Deprivation Therapy in Murine Prostate Tumors," *Journal for Immunotherapy of Cancer* 12 (2024): e008760, https://doi.org/10.1136/jitc-2023-008760.

32. Y. J. Chang, C. H. Chang, T. J. Chang, et al., "Biodistribution, Pharmacokinetics and microSPECT/CT Imaging of 188Re-bMEDA-Liposome in a C26 Murine Colon Carcinoma Solid Tumor Animal Model," *Anticancer Research* 27 (2007): 2217–2225.

33. M. H. Chen, C. H. Chang, Y. J. Chang, et al., "MicroSPECT/CT Imaging and Pharmacokinetics of 188Re-(DXR)-Liposome in Human Colorectal Adenocarcinoma-Bearing Mice," *Anticancer Research* 30 (2010): 65–72.

34. Y. Wang, R. Barmin, F. M. Mottaghy, F. Kiessling, T. Lammers, and R. M. Pallares, "Nanoparticles in Nuclear Medicine: From Diagnostics to Therapeutics," *Journal of Controlled Release* 383 (2025): 113815, https://doi.org/10.1016/j.jconrel.2025.113815.

35. B. P. Riff, Y.-X. Yang, M. C. Soulen, et al., "Peptide Receptor Radionuclide Therapy–Induced Hepatotoxicity in Patients With Metastatic Neuroendocrine Tumors," *Clinical Nuclear Medicine* 40 (2015): 845–850, https://doi.org/10.1097/RLU.0000000000000935.

36. K. Herrmann, M. Schwaiger, J. S. Lewis, et al., "Radiotheranostics: A Roadmap for Future Development," *Lancet Oncology* 21 (2020): e146–e156, https://doi.org/10.1016/S1470-2045(19)30821-6.

37. M. Silindir-Gunay and N. Ozolmez, "Adverse Reactions to Therapeutic Radiopharmaceuticals," *Applied Radiation and Isotopes* 214 (2024): 111527, https://doi.org/10.1016/j.apradiso.2024.111527.

38. C. I. Colino, J. M. Lanao, and C. Gutierrez-Millan, "Targeting of Hepatic Macrophages by Therapeutic Nanoparticles," *Frontiers in Immunology* 11 (2020): 218, https://doi.org/10.3389/fimmu.2020.00218.

39. C. T. Inglut, A. J. Sorrin, T. Kuruppu, et al., "Immunological and Toxicological Considerations for the Design of Liposomes," *Nanomaterials (Basel)* 10 (2020): 190, https://doi.org/10.3390/nano10020190.

40. C. Stavnsbjerg, E. Christensen, R. Münter, et al., "Accelerated Blood Clearance and Hypersensitivity by PEGylated Liposomes Containing TLR Agonists," *Journal of Controlled Release* 342 (2022): 337–344, https://doi.org/10.1016/j.jconrel.2021.12.033.

41. M. Asoudeh, N. Nguyen, M. Raith, et al., "PEGylated Nanoparticles Interact With Macrophages Independently of Immune Response Factors and Trigger a Non-Phagocytic, Low-Inflammatory Response," *Journal of Controlled Release* 366 (2024): 282–296, https://doi.org/10.1016/j.jconrel.2023.12.019.

42. J. E. Bader, R. T. Enos, K. T. Velázquez, et al., "Repeated Clodronate-Liposome Treatment Results in Neutrophilia and Is Not Effective in Limiting Obesity-Linked Metabolic Impairments," *American Journal of Physiology. Endocrinology and Metabolism* 316 (2019): E358–E372, https://doi.org/10.1152/ajpendo.00438.2018.

43. B. Beck-Schimmer, R. Schwendener, T. Pasch, L. Reyes, C. Booy, and R. C. Schimmer, "Alveolar Macrophages Regulate Neutrophil Recruitment in Endotoxin-Induced Lung Injury," *Respiratory Research* 6 (2005): 61, https://doi.org/10.1186/1465-9921-6-61.

44. H. H. Lee, L. Aslanyan, A. Vidyasagar, et al., "Depletion of Alveolar Macrophages Increases Pulmonary Neutrophil Infiltration, Tissue Damage, and Sepsis in a Murine Model of *Acinetobacter baumannii* Pneumonia," *Infection and Immunity* 88 (2020): e00128-20, https://doi.org/10.1128/iai.00128-20.

45. F. Y. J. Huang, T. W. Lee, C. H. K. Kao, et al., "Imaging, Autoradiography, and Biodistribution of 188Re-Labeled PEGylated Nanoliposome in Orthotopic Glioma Bearing Rat Model," *Cancer Biotherapy & Radiopharmaceuticals* 26 (2011): 717–725, https://doi.org/10.1089/cbr.2011.1052.

46. C. M. Liu, W. C. Lee, C. Y. Yu, et al., "Comparison of the Therapeutic Efficacy of 188Rhenium-Liposomes and Liposomal Doxorubicin in a 4T1 Murine Orthotopic Breast Cancer Model," *Oncology Reports* 27 (2012): 678–684, https://doi.org/10.3892/or.2011.1557.

47. S. J. Hong, T. H. Ahn, W. J. Shim, et al., "Macrophage Depletion by Clodronate Liposomes Suppresses Neointimal Formation After Carotid Artery Injury in Apolipoprotein E-Deficient Mice," *Korean Circulation Journal* 38 (2008): 244–249, https://doi.org/10.4070/kcj.2008.38.5.244.

48. S. Y. Liu, W. C. Huang, H. I. Yeh, et al., "Sequential Blockade of PD-1 and PD-L1 Causes Fulminant Cardiotoxicity—From Case Report to Mouse Model Validation," *Cancers (Basel)* 11 (2019): 580, https://doi.org/10.3390/cancers11040580.

49. C. H. Chang, M. C. Chang, Y. J. Chang, L. C. Chen, T. W. Lee, and G. Ting, "Translating Research for the Radiotheranostics of Nanotargeted 188Re-Liposome," *International Journal of Molecular Sciences* 22 (2021): 3868, https://doi.org/10.3390/ijms22083868.

50. C. L. Scott, S. Henri, and M. Guilliams, "Mononuclear Phagocytes of the Intestine, the Skin, and the Lung," *Immunological Reviews* 262 (2014): 9–24, https://doi.org/10.1111/imr.12220.

51. S. Gordon, A. Roberti, and S. H. E. Kaufmann, "Mononuclear Phagocytes, Cellular Immunity, and Nobel Prizes: A Historic Perspective," *Cells* 13 (2024): 1378, https://doi.org/10.3390/cells13161378.

52. S. Culemann, K. Knab, M. Euler, et al., "Stunning of Neutrophils Accounts for the Anti-Inflammatory Effects of Clodronate Liposomes," *Journal of Experimental Medicine* 220 (2023): e20220525, https://doi.org/10.1084/jem.20220525.

53. N. L. Ward, C. M. Loyd, J. A. Wolfram, D. Diaconu, C. M. Michaels, and T. S. McCormick, "Depletion of Antigen Presenting Cells by Clodronate Liposomes Reverses the Psoriatic Skin Phenotype in KC-Tie2 Mice," *British Journal of Dermatology* 164 (2011): 750–758, https://doi.org/10.1111/j.1365-2133.2010.10129.x.

54. A. Vito, S. Rathmann, N. Mercanti, N. el-Sayes, K. Mossman, and J. Valliant, "Combined Radionuclide Therapy and Immunotherapy for Treatment of Triple Negative Breast Cancer," *International Journal of Molecular Sciences* 22 (2021): 4843, https://doi.org/10.3390/ijms22094843.

55. H. K. Potluri, C. A. Ferreira, J. Grudzinski, et al., "Antitumor Efficacy of 90Y-NM600 Targeted Radionuclide Therapy and PD-1 Blockade Is Limited by Regulatory T Cells in Murine Prostate Tumors," *Journal for Immunotherapy of Cancer* 10 (2022): e005060, https://doi.org/10.1136/jitc-2022-005060.

56. R. Hernandez, K. L. Walker, J. J. Grudzinski, et al., "90Y-NM600 Targeted Radionuclide Therapy Induces Immunologic Memory in Syngeneic Models of T-Cell Non-Hodgkin's Lymphoma," *Communications Biology* 2 (2019): 79, https://doi.org/10.1038/s42003-019-0327-4.

57. Y. Wu, A. K. Pfeifer, R. Myschetzky, et al., "Induction of Anti-Tumor Immune Responses by Peptide Receptor Radionuclide Therapy With 177Lu-DOTATATE in a Murine Model of a Human Neuroendocrine Tumor," *Diagnostics* 3 (2013): 344–355, https://doi.org/10.3390/diagnostics3040344.

58. E. Zhang, C. Ding, S. Li, et al., "Roles and Mechanisms of Tumour-Infiltrating B Cells in Human Cancer: A New Force in Immunotherapy," *Biomarker Research* 11 (2023): 28, https://doi.org/10.1186/s40364-023-00460-1.

59. A. Hegoburu, M. Amer, F. Frizelle, and R. Purcell, "B Cells and Tertiary Lymphoid Structures in Cancer Therapy Response," *BJC Reports* 3 (2025): 40, https://doi.org/10.1038/s44276-025-00146-1.

60. H. Yang, Z. Zhang, J. Li, K. Wang, W. Zhu, and Y. Zeng, "The Dual Role of B Cells in the Tumor Microenvironment: Implications for Cancer Immunology and Therapy," *International Journal of Molecular Sciences* 25 (2024): 11825, https://doi.org/10.3390/ijms252111825.

61. J. Chen, Y. Zhou, Y. Pang, et al., "FAP-Targeted Radioligand Therapy With 68Ga/177Lu-DOTA-2P(FAPI)2 Enhance Immunogenicity and Synergize With PD-L1 Inhibitors for Improved Antitumor Efficacy," *Journal for Immunotherapy of Cancer* 13 (2025): e010212, https://doi.org/10.1136/jitc-2024-010212.

62. N. A. Kaya, D. Tai, X. Lim, et al., "Multimodal Molecular Landscape of Response to Y90-Resin Microsphere Radioembolization Followed by Nivolumab for Advanced Hepatocellular Carcinoma," *Journal for Immunotherapy of Cancer* 11 (2023): e007106, https://doi.org/10.1136/jitc-2023-007106.

63. M. Luna-Gutiérrez, E. Azorín-Vega, R. Oros-Pantoja, et al., "Lutetium-177 Labeled iPD-L1 as a Novel Immunomodulator for Cancer-Targeted Radiotherapy," *EJNMMI Radiopharmacy and Chemistry* 10 (2025): 5, https://doi.org/10.1186/s41181-025-00328-9.

64. R. Neta and J. J. Oppenheim, "Radioprotection With Cytokines—Learning From Nature to Cope With Radiation Damage," *Cancer Cells* 3 (1991): 391–396.

65. M. Dougan, G. Dranoff, and S. K. Dougan, "GM-CSF, IL-3, and IL-5 Family of Cytokines: Regulators of Inflammation," *Immunity* 50 (2019): 796–811, https://doi.org/10.1016/j.immuni.2019.03.022.

66. C. P. Kerr, J. J. Grudzinski, T. P. Nguyen, R. Hernandez, J. P. Weichert, and Z. S. Morris, "Developments in Combining Targeted Radionuclide Therapies and Immunotherapies for Cancer Treatment," *Pharmaceutics* 15 (2023): 128, https://doi.org/10.3390/pharmaceutics15010128.

67. S. C. Kleinendorst, E. Oosterwijk, J. Bussink, H. Westdorp, M. W. Konijnenberg, and S. Heskamp, "Combining Targeted Radionuclide Therapy and Immune Checkpoint Inhibition for Cancer Treatment," *Clinical Cancer Research* 28 (2022): 3652–3657, https://doi.org/10.1158/1078-0432.CCR-21-4332.

68. B. Benner, L. Good, D. Quiroga, et al., "Pexidartinib, a Novel Small Molecule CSF-1R Inhibitor in Use for Tenosynovial Giant Cell Tumor: A Systematic Review of Pre-Clinical and Clinical Development," *Drug Design, Development and Therapy* 14 (2020): 1693–1704, https://doi.org/10.2147/DDDT.S253232.

69. A. Povo-Retana, M. Fariñas, R. Landauro-Vera, et al., "Immunometabolic Actions of Trabectedin and Lurbinectedin on Human Macrophages: Relevance for Their Anti-Tumor Activity," *Frontiers in Immunology* 14 (2023): 1211068, https://doi.org/10.3389/fimmu.2023.1211068.

Supporting Information

Additional supporting information can be found online in the Supporting Information section. **Figure S1:** Modulation of immune cell populations by Lipo-Re188 following macrophage depletion. (A) Quantification of B cells (A), PMN-MDSC and M-MDSC (B) among $CD45^+$ splenocytes in each treatment group ($n = 3$). Quantification of B cells (C), PMN-MDSC and M-MDSC (D), NK cells and NKT cells (E) among $CD45^+$ cells in the TME ($n = 3$). Data are presented as mean ± SD. Statistical significance was determined using one-way ANOVA with Tukey's post hoc test. $^*p < 0.05$; $^{**}p < 0.01$; $^{***}p < 0.001$; $^{****}p < 0.0001$. **Figure S2:** Lipo-Re188 upregulates Ly6G and PD-L1 expression in the spleen. Representative flow cytometry plots (A) and quantification of $Ly6G^+$ cells (B) in the spleen from control, liposome, and Lipo-Re188 groups on day 5 post-treatment ($n = 3$). Representative flow cytometry plots (C) and quantification of PD-L1 expression (D) in splenic cells from control, liposome, and Lipo-Re188 groups on day 5 post-treatment ($n = 3$). Data are presented as mean ± SD. Statistical significance was determined using one-way ANOVA with Tukey's post hoc test. $^*p < 0.05$; $^{**}p < 0.01$. **Figure S3:** Immune profiling after triple combination therapy with Lipo-clod, Lipo-Re188, and PD-L1 blockade in a lung metastasis model. Quantification of $CD4^+$ and $CD8^+$ T cells (A) and PMN-MDSC and M-MDSC (B) among $CD45^+$ splenocytes in each treatment group ($n = 3$). Quantification of $CD4^+$ and $CD8^+$ T cells (C), PMN-MDSC and M-MDSC (D) among $CD45^+$ cells in the TME ($n = 3$). Data are presented as mean ± SD. Statistical significance was determined using one-way ANOVA with Tukey's post hoc test. $^*p < 0.05$; $^{**}p < 0.01$; $^{***}p < 0.001$; $^{****}p < 0.0001$.